CHANGE DETECTION IN THE 1996-1997 AVHRR OCEANS PATHFINDER SEA SURFACE TEMPERATURE DATA

Allan A. Nielsen[1], *Knut Conradsen*[1] *and Ole B. Andersen*[2]

[1]Informatics and Mathematical Modelling, Technical University of Denmark, Building 321
DK-2800 Kgs. Lyngby, Denmark
aa@imm.dtu.dk, www.imm.dtu.dk/∼aa
[2]Danish National Survey and Cadastre, Rentemestervej 8
DK-2400 Copenhagen NV, Denmark
oa@kms.dk, www.kms.dk

ABSTRACT

This paper describes the application of orthogonal transformations to detect the El Niño/Southern Oscillation (ENSO) built-up and other ocean related phenomena by detecting the multivariate change in the monthly mean sea surface temperature (SST) as given by the NOAA/NASA AVHRR Oceans Pathfinder data. The transforms applied include canonical correlations analysis based multivariate alteration detection (MAD) variates and maximum autocorrelation factors (MAFs). The results show that the large scale ocean events associated with ENSO related changes are concentrated in the first MAFs of MADs.

1. INTRODUCTION

This paper deals with detection of non-trivial change in multivariate, bi-temporal data. The term "non-trivial change" here means non-affine change between two points in time, i.e., change due to for instance an additive shift in mean level (offset) or a multiplicative shift in calibration of a measuring device (gain) is not detected.

The method applied which is called multivariate alteration detection (MAD) [9, 11, 12] is based on the established multivariate statistical technique canonical correlations analysis (CCA) [8] and post-processing by the maximum autocorrelation factors (MAF) transformation [16, 7]. Here, the method is applied to detect change in the 1996-1997 AVHRR Oceans Pathfinder sea surface temperature data. The method is reported with other case studies in [9, 12, 10].

Analysis of multi-temporal oceanographic data is often performed by means of empirical orthogonal functions (EOFs) as described in [14]. The analysis carried out here can be considered as an extension to the usual EOF analysis.

This work was carried out in the GEOSONAR project funded by the Danish Research Councils' Earth Observation Programme. The GEOSONAR homepage is http://manicoral.kms.dk/PK/geosonar.html.

2. METHODS

When analysing changes in panchromatic images taken at different points in time it is customary to analyse the difference between two images, possibly after some normalisation. The idea is of course that areas with no or little change have zero or low absolute values and areas with large changes have large absolute values in the difference image. If we have two multivariate images with variables at a given location written as vectors (without loss of generality we assume that $\mathrm{E}\{\boldsymbol{X}\} = \mathrm{E}\{\boldsymbol{Y}\} = \boldsymbol{0}$)

$$\boldsymbol{X} = [X_1 \ \ldots \ X_k]^T \quad \text{and} \quad \boldsymbol{Y} = [Y_1 \ \ldots \ Y_k]^T \tag{1}$$

where k is the number of spectral bands, then a simple change detection transformation is

$$\boldsymbol{X} - \boldsymbol{Y} = [X_1 - Y_1 \ \ldots \ X_k - Y_k]^T. \tag{2}$$

If our image data have more than three channels it is difficult to visualise change in all channels simultaneously. To overcome this problem and to concentrate information on change, linear transformations of the image data that optimise some design criterion can be considered. A linear transformation that will maximise a measure of change in the simple multispectral difference image is one that maximises deviations from no change for instance the variance

$$\mathrm{Var}\{v_1(X_1 - Y_1) + \cdots + v_k(X_k - Y_k)\} = \mathrm{Var}\{\boldsymbol{v}^T(\boldsymbol{X} - \boldsymbol{Y})\}. \tag{3}$$

Areas in the image data with high absolute values of $\boldsymbol{v}^T(\boldsymbol{X} - \boldsymbol{Y})$ are maximum change areas. A multiplication of vector $\boldsymbol{v}$ with a constant c will multiply the variance with c^2. Therefore we must make a choice concerning $\boldsymbol{v}$. A natural choice is to request that $\boldsymbol{v}$ is a unit vector, $\boldsymbol{v}^T\boldsymbol{v} = 1$. This amounts to finding principal components of the simple difference images.

A more parameter rich measure of change that allows different coefficients for $\boldsymbol{X}$ and $\boldsymbol{Y}$ and different numbers of

spectral bands in the two sets, p and q respectively ($p \leq q$), are linear combinations

$$\boldsymbol{a}^T\boldsymbol{X} = a_1X_1 + \cdots + a_pX_p \quad (4)$$
$$\boldsymbol{b}^T\boldsymbol{Y} = b_1Y_1 + \cdots + b_qY_q \quad (5)$$

and the difference between them $\boldsymbol{a}^T\boldsymbol{X} - \boldsymbol{b}^T\boldsymbol{Y}$. This measure also accounts for situations where the spectral bands are not the same but cover different spectral regions, for instance if one set of data comes from Landsat MultiSpectral Scanner (MSS) and the other set comes from Landsat Thematic Mapper (TM) or from SPOT High Resolution Visible (HRV) which may be valuable in historical terrestrial change studies. In this case one must be more cautious when interpreting the multivariate difference as multivariate change.

To find $\boldsymbol{a}$ and $\boldsymbol{b}$ [5] uses principal components (PC) analysis on $\boldsymbol{X}$ and $\boldsymbol{Y}$ considered as one concatenated vector variable. [6] applies PC analysis to simple difference images as described above. The approach suggested in [5] defines $\boldsymbol{a}$ and $\boldsymbol{b}$ simultaneously but the method does not have a clear design criterion. Also, bands are treated similarly whether or not they come from different points in time. The approach suggested in [6] depends on the scale at which the individual variables are measured (for instance it depends on gain settings of a measuring device). Also, it forces the two sets of variables to have the same coefficients (with opposite sign), and it does not allow for the case where the two sets of images have different numbers of channels. A potentially better approach is to define a set of $\boldsymbol{a}$ and $\boldsymbol{b}$ simultaneously in the fashion described below. Again, let us maximise the variance, this time $\mathrm{Var}\{\boldsymbol{a}^T\boldsymbol{X} - \boldsymbol{b}^TY\}$. A multiplication of $\boldsymbol{a}$ and $\boldsymbol{b}$ with a constant c will multiply the variance with c^2. Therefore we must make choices concerning $\boldsymbol{a}$ and $\boldsymbol{b}$, and natural choices in this case are requesting unit variance of $\boldsymbol{a}^T\boldsymbol{X}$ and $\boldsymbol{b}^T\boldsymbol{Y}$. The criterion then is: maximise $\mathrm{Var}\{\boldsymbol{a}^T\boldsymbol{X} - \boldsymbol{b}^T\boldsymbol{Y}\}$ with $\mathrm{Var}\{\boldsymbol{a}^T\boldsymbol{X}\} = \mathrm{Var}\{\boldsymbol{b}^T\boldsymbol{Y}\} = 1$. With this choice we have

$$\begin{aligned}&\mathrm{Var}\{\boldsymbol{a}^T\boldsymbol{X} - \boldsymbol{b}^T\boldsymbol{Y}\} \quad (6)\\ &= \mathrm{Var}\{\boldsymbol{a}^T\boldsymbol{X}\} + \mathrm{Var}\{\boldsymbol{b}^T\boldsymbol{Y}\} - 2\mathrm{Cov}\{\boldsymbol{a}^T\boldsymbol{X}, \boldsymbol{b}^T\boldsymbol{Y}\}\\ &= 2(1 - \mathrm{Corr}\{\boldsymbol{a}^T\boldsymbol{X}, \boldsymbol{b}^T\boldsymbol{Y}\}).\end{aligned}$$

We shall request that $\boldsymbol{a}^T\boldsymbol{X}$ and $\boldsymbol{b}^T\boldsymbol{Y}$ are positively correlated. Therefore, determining the difference between linear combinations with maximum variance corresponds to determining linear combinations with minimum (non-negative) correlation. Determination of linear combinations with extreme correlations brings the theory of canonical correlations analysis to mind.

2.1. Canonical Correlations Analysis, CCA

Canonical correlations analysis investigates the relationship between two groups of variables. It finds two sets of linear combinations of the original variables, one for each group. The first two linear combinations are the ones with the largest correlation. This correlation is called the first canonical correlation and the two linear combinations are called the first canonical variates. The second two linear combinations are the ones with the largest correlation subject to the condition that they are orthogonal to the first canonical variates. This correlation is called the second canonical correlation and the two linear combinations are called the second canonical variates. Higher order canonical correlations and canonical variates are defined similarly.

If we denote the dispersion or covariance matrix of the one set of variables ($\boldsymbol{X}$) $\boldsymbol{\Sigma}_{11}$, the dispersion of the other set of variables ($\boldsymbol{Y}$) $\boldsymbol{\Sigma}_{22}$, the covariance between them $\boldsymbol{\Sigma}_{12}$, and the canonical correlation ρ then we get

$$\rho^2 = \frac{\boldsymbol{a}^T\boldsymbol{\Sigma}_{12}\boldsymbol{\Sigma}_{22}^{-1}\boldsymbol{\Sigma}_{21}\boldsymbol{a}}{\boldsymbol{a}^T\boldsymbol{\Sigma}_{11}\boldsymbol{a}} = \frac{\boldsymbol{b}^T\boldsymbol{\Sigma}_{21}\boldsymbol{\Sigma}_{11}^{-1}\boldsymbol{\Sigma}_{12}\boldsymbol{b}}{\boldsymbol{b}^T\boldsymbol{\Sigma}_{22}\boldsymbol{b}} \quad (7)$$

or

$$\boldsymbol{\Sigma}_{12}\boldsymbol{\Sigma}_{22}^{-1}\boldsymbol{\Sigma}_{21}\boldsymbol{a} = \rho^2\boldsymbol{\Sigma}_{11}\boldsymbol{a} \quad (8)$$
$$\boldsymbol{\Sigma}_{21}\boldsymbol{\Sigma}_{11}^{-1}\boldsymbol{\Sigma}_{12}\boldsymbol{b} = \rho^2\boldsymbol{\Sigma}_{22}\boldsymbol{b} \quad (9)$$

i.e., we find the desired projections for $\boldsymbol{X}$ by considering the conjugate eigenvectors $\boldsymbol{a}_1, \ldots, \boldsymbol{a}_p$ corresponding to the eigenvalues $\rho_1^2 \geq \cdots \geq \rho_p^2 \geq 0$ of $\boldsymbol{\Sigma}_{12}\boldsymbol{\Sigma}_{22}^{-1}\boldsymbol{\Sigma}_{21}$ with respect to $\boldsymbol{\Sigma}_{11}$. Similarly, we find the desired projections for $\boldsymbol{Y}$ by considering the conjugate eigenvectors $\boldsymbol{b}_1, \ldots, \boldsymbol{b}_p$ of $\boldsymbol{\Sigma}_{21}\boldsymbol{\Sigma}_{11}^{-1}\boldsymbol{\Sigma}_{12}$ with respect to $\boldsymbol{\Sigma}_{22}$ corresponding to the same eigenvalues ρ_i^2.

This technique was first described in [8] and a treatment is given in most textbooks on multivariate statistics (good references are [4, 2]).

[18] deals with (iterated) PC analysis of the same variable at the two points in time and consider the second PC as a (marginal) change detector for that variable. [18] also introduces spatial measures such as inverse local variance weighting in statistics calculation and Markov random field modelling of the probability of change (vs. no change).

2.2. The MAD Transformation

In accordance with the above we define the multivariate alteration detection (MAD) transformation as

$$\begin{bmatrix}\boldsymbol{X}\\ \boldsymbol{Y}\end{bmatrix} \rightarrow [\boldsymbol{a}_p^T\boldsymbol{X} - \boldsymbol{b}_p^T\boldsymbol{Y} \ \ldots \ \boldsymbol{a}_1^T\boldsymbol{X} - \boldsymbol{b}_1^T\boldsymbol{Y}]^T \quad (10)$$

where $\boldsymbol{a}_i$ and $\boldsymbol{b}_i$ are the defining coefficients from a standard canonical correlations analysis. $\boldsymbol{X}$ and $\boldsymbol{Y}$ are vectors with $\mathrm{E}\{\boldsymbol{X}\} = \mathrm{E}\{\boldsymbol{Y}\} = \boldsymbol{0}$. The dispersion matrix of the MAD variates is

$$\mathrm{D}\{\boldsymbol{a}^T\boldsymbol{X} - \boldsymbol{b}^T\boldsymbol{Y}\} = 2(\boldsymbol{I} - \boldsymbol{R}) \quad (11)$$

where $\boldsymbol{I}$ is the $p\times p$ unit matrix and $\boldsymbol{R}$ is a $p\times p$ matrix containing the sorted canonical correlations on the diagonal and zeros off the diagonal.

The MAD transformation has the very important property that if we consider linear combinations of two sets of p respectively q $(p \leq q)$ variables that are positively correlated then the pth difference shows maximum variance among such variables. The $(p-j)$th difference shows maximum variance subject to the constraint that this difference is uncorrelated with the previous j ones. In this way we may sequentially extract uncorrelated difference images where each new image shows maximum difference (change) under the constraint of being uncorrelated with the previous ones. If $p < q$ then the projection of $\boldsymbol{Y}$ on the eigenvectors corresponding to the eigenvalues 0 will be independent of $\boldsymbol{X}$. That part may be considered the extreme case of multivariate change detection. As opposed to the principal components of simple differences the MAD variates are invariant to affine transformations (including linear scaling), which means that they are not sensitive to for example gain settings of a measuring device, and to linear radiometric and atmospheric correction schemes.

2.3. The MAF Transformation

To find maximum change areas with high spatial autocorrelation a MAF post-processing of the MAD variates is suggested. The MAF transformation can be considered as a spatial extension of PC analysis in which the new variates maximise autocorrelation between neighbouring pixels rather than variance (as with PCs). MAF analysis corresponds to CCA between multivariate image data and the same image data spatially shifted. Also the MAF transformation is invariant to affine transformations (including linear scaling).

3. DATA

The data used in the case study come from the NOAA/NASA AVHRR Oceans Pathfinder SST dataset maintained and made available by PO.DAAC at JPL, California, USA. NOAA is the National Oceanographic and Atmospheric Administration, NASA is the National Aeronautics and Space Administration, AVHRR, the Advanced Very High Resolution Radiometer, is a multispectral instrument on board a series of NOAA satellites, SST is sea surface temperature, PO.DAAC is the Physical Oceanography Distributed Active Archive Center, and JPL is the Jet Propulsion Laboratory. More specifically, the data used are the global equal-angle best SST monthly mean values of the daytime (ascending) 0.5 degree (54 km) data [13].

Based on radiative transfer theory the satellite data are calibrated to temperatures that are nominally accurate to 0.3°C [3].

4. RESULTS AND DISCUSSION

For space constraint reasons neither the original monthly mean SST for 1996 and 1997 nor the monthly mean SST anomalies for 1996 and 1997 with the temporal mean subtracted are shown. Fig. 1 shows the difference of monthly mean SST for 1996 and 1997 ("1997 minus 1996") stretched linearly between –10.0 °C and 10.0°C.

The statistics calculations for the data transformations are carried out only where all 24 months have valid data for SST. Figs. 2 and 3 show the MADs and the MAF/MADs stretched linearly between mean ∓ 3 standard deviations. Here the 1996 data are considered as 12 variables ($\boldsymbol{X}$ in Eq. 10) and the 1997 data are considered as 12 variables ($\boldsymbol{Y}$ in Eq. 10). Fig. 4 shows the correlations between the the monthly mean SST for 1996 and 1997 and the MAF/-MADs. Due to space limitations no other images or details from the statistical analysis are shown.

Due to the great variation in mean temperature ranging more than 30°C between the poles and the Equator more or less no other variations in SST are visible—not even seasonal or El Niño Southern Oscillation (ENSO) related signals.

By considering the twelve 1996 monthly mean SST as 12 variables from one point in time and the twelve 1997 monthly mean SST as 12 variables from another point in time, the analysis focuses on inter-annual changes in SST. Consequently the annual signal which corresponds to the largest variation SST is suppressed. By forming the 12 monthly averaged SST differences between 1997 and 1996, as presented in Fig. 1, inter-annual variations become visible. Large scale changes related to the ENSO signal are clearly seen, but also differences in the North Sea, Baltic regions during June and July can be seen. Similarly, differences in the Mediterranean Sea during September and October, and along the west coast of the USA during June through December are visible in the differences in Fig. 1.

In 1997 and 1998, one of the largest ENSO events on record in the Pacific Ocean occurred, with the onset in mid-1997 leading to a peak in early 1998 following the characterisation in [15]. The onset is clearly seen in the simple differences in Fig. 1 starting in May 1997 and increasing throughout the rest of the year.

Fig. 2 shows the MADs of the 1996-1997 monthly AVHRR mean SST. The largest variance captured in MAD 1 is found in coastal areas, and also in the Mediterranean Sea, however these structures have very limited spatial extend. In most of the twelve MADs, structures related to the ENSO can be found, but these are most dominant in MADs 9-12. The correlations over time between the 1996-1997 SSTs and the MADs (not shown) indicate relatively short period signals for the first MADs, whereas long period structures being increasingly trend-like are seen for MADs 9-12 which are the MADs dominated by the ENSO event.

Upon transforming the MADs via MAF (Fig. 3) creating change variables which have maximum autocorrelation between neighbouring pixels, change features of largest spatial extend are isolated in MAF 1, and so forth in the higher order MAFs. Whereas any physical interpretation is diffi-

cult using the MADs, the MAFs of the MADs exhibit more physical realism and more ease of interpretation. Features of large spatial autocorrelation like the ENSO signal concentrate in the first MAFs as seen in Fig. 3. In the MADs the large scale increased surface temperatures in 1997 in the eastern part of the Pacific Ocean were found in MADs 9-12. Similarly, the correlations in MAF/MAD 1 between the 1996-1997 SSTs in Fig. 4 are very high but with opposite signs for the two years indicating a shift or trend-like structure for this MAF, se also [1]. One further finding in MAF 1 is the apparent basin scale opposite SST signature to the ENSO event in the South Atlantic Ocean. As years adjacent to 1996 and 1997 have not been studied it is difficult to establish whether either 1996 or 1997 was anomalous. However, recalling that seasonal upwelling along the coast of Ghana and the Ivory Coast is most likely the result of remote wind forcing and Kelvin wave propagation along the Equator, it is likely that the El Niño mechanism may be as important to the Atlantic as it is to the Pacific [17].

Most other MAFs are seen to have structure in the Pacific that ressembles the structure of the Intertropical Convergence Zone and the South Pacific Convergence Zone, and consequently being related to the ENSO dynamics. Similarly dynamics related to the Antarctic Circumpolar Current are clearly seen in MAFs 2 and 3 and several higher order MAFs. Here the correlations between the 1996 and 1997 (Fig. 4) are also changing on monthly scales indicating that the differences stem from dynamically active areas.

MAF 1 also contains some significant signals in the northern-most parts of the North Atlantic Ocean. These structures should most likely be found in higher order MAFs, but appear in MAF 1 probably due to the spherical shape of the Earth which means that a one degree longitude band narrows with the cosine to the latitude, such that one degree longitude corresponds to 110 km at the Equator, but only 50 km at 65 degrees decreasing towards the pole.

5. ACKNOWLEDGMENTS

The NOAA/NASA AVHRR Oceans Pathfinder SST database provision at JPL is due to Jorge Vazquez, Rosanna Sumagaysay and co-workers.

6. REFERENCES

[1] O. A. Andersen and P. Knudsen. Regional sea surface height and temperature trends from ERS satellites. In *Proceedings of the ERS-ENVISAT Symposium*, Gothenburg, Sweden, 2000.

[2] T. W. Anderson. *An Introduction to Multivariate Statistical Analysis*. John Wiley, New York, second edition, 1984.

[3] J. W. Brown, O. B. Brown, and R. H. Evans. Calibration of AVHRR infraread channels: A new approach to non-linear correction. *Journal of Geophysical Research*, 98(NC10), 1993.

[4] W. W. Cooley and P. R. Lohnes. *Multivariate Data Analysis*. John Wiley and Sons, New York, 1971.

[5] T. Fung and E. LeDrew. Application of principal components analysis to change detection. *Photogrammetric Engineering and Remote Sensing*, 53(12):1649–1658, 1987.

[6] P. Gong. Change detection using principal component analysis and fuzzy set theory. *Canadian Journal of Remote Sensing*, 19(1):22–29, 1993.

[7] A. A. Green, M. Berman, P. Switzer, and M. D. Craig. A transformation for ordering multispectral data in terms of image quality with implications for noise removal. *IEEE Transactions on Geoscience and Remote Sensing*, 26(1):65–74, 1988.

[8] H. Hotelling. Relations between two sets of variates. *Biometrika*, XXVIII:321–377, 1936.

[9] A. A. Nielsen. *Analysis of Regularly and Irregularly Sampled Spatial, Multivariate, and Multi-temporal Data*. PhD thesis, Department of Mathematical Modelling, Technical University of Denmark, Lyngby, 1994. Internet http://www.imm.dtu.dk/∼aa/phd/.

[10] A. A. Nielsen. Multi-channel remote sensing data and orthogonal transformations for change detection. In I. Kanellopoulos, G. G. Wilkinson, and T. Moons, editors, *Machine Vision and Advanced Image Processing in Remote Sensing*. Springer, 1999.

[11] A. A. Nielsen and K. Conradsen. Multivariate Alteration Detection (MAD) in Multispectral, Bi-temporal Image Data: A New Approach to Change Detection Studies. Technical Report 1997-11, Department of Mathematical Modelling, Technical University of Denmark, Lyngby, 1997. Internet http://www.imm.dtu.dk/∼aa/tech-rep-1997-11/.

[12] A. A. Nielsen, K. Conradsen, and J. J. Simpson. Multivariate alteration detection (MAD) and MAF post-processing in multispectral, bi-temporal image data: New approaches to change detection studies. *Remote Sensing of Environment*, 64:1–19, 1998.

[13] PO.DAAC. http://podaac.jpl.nasa.gov. Jet Propulsion Laboratory, National Aeronautics and Space Administration, Pasadena, California, USA.

[14] R. W. Preisendorfer. *Principal Component Analysis in Meteorology and Oceanography*. Posthumously compiled and edited by C. D. Morley. Developments in Atmospheric Science, 17, Elsevier, 1988.

[15] E. M. Rasmusson and T. H. Carpenter. Variations in tropical sea surface temperature and surface wind field associated with the Southern Ocean/El Niño. *Monthly Weather Review*, 110:354–384, 1982.

[16] P. Switzer and A. A. Green. Min/max autocorrelation factors for multivariate spatial imagery. Technical Report 6, Department of Statistics, Stanford University, 1984.

[17] M. Tomczak and J. S. Godfrey. *Regional Oceanography: An Introduction*. Oxford, 1994.

[18] R. Wiemker, A. Speck, D. Kulbach, H. Spitzer, and J. Beinlein. Unsupervised robust change detection in multispectral imagery using spectral and spatial features. In *Proceedings from the Second International Airborne Remote Sensing Conference and Exhibition, Vol. I*, pages 640–647, Copenhagen, Denmark, 1997.

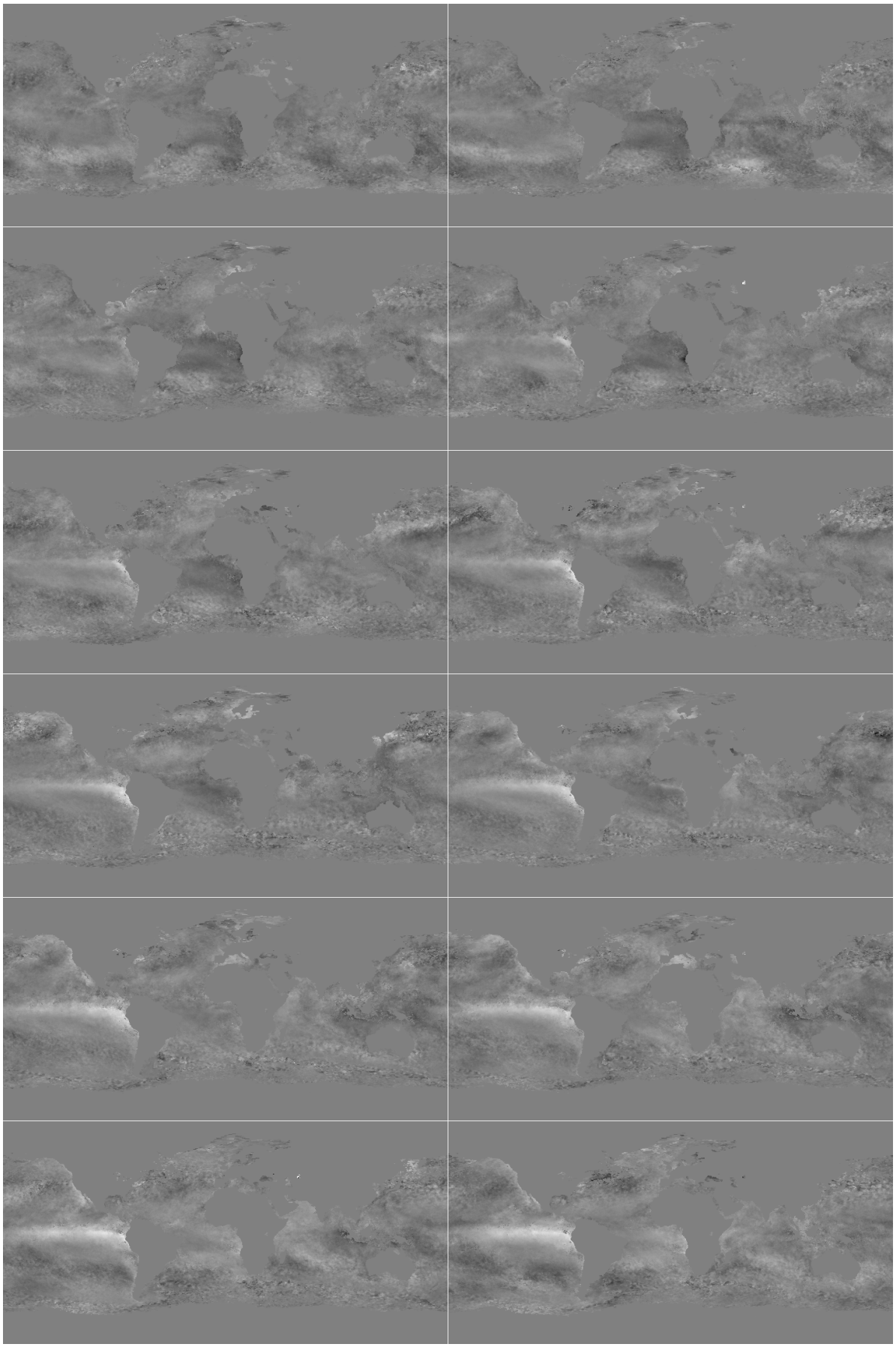

Fig. 1. Simple differences of 1996-1997 AVHRR monthly mean SST (“1997 minus 1996”)

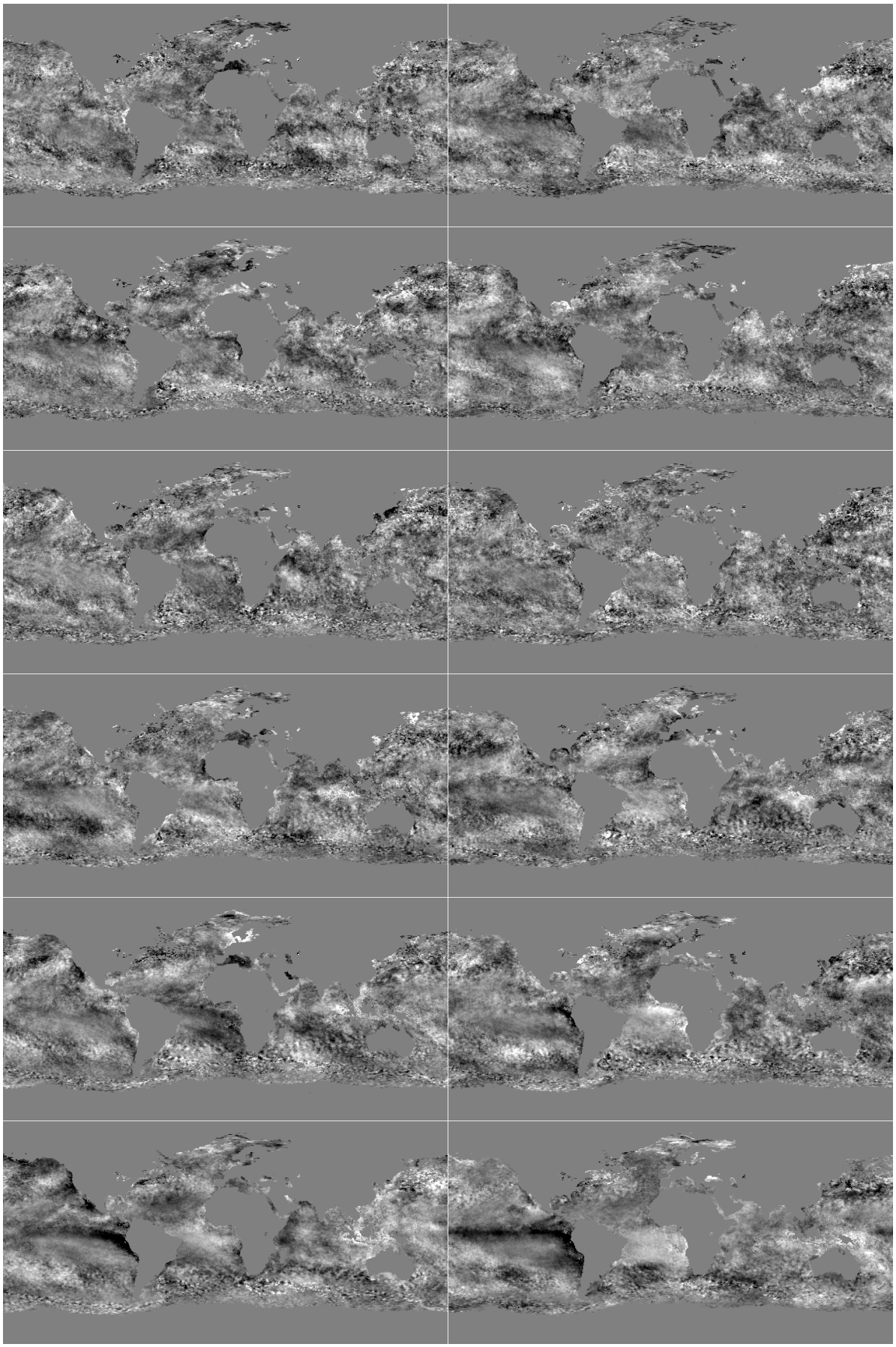

Fig. 2. MADs of 1996-1997 AVHRR monthly mean SST

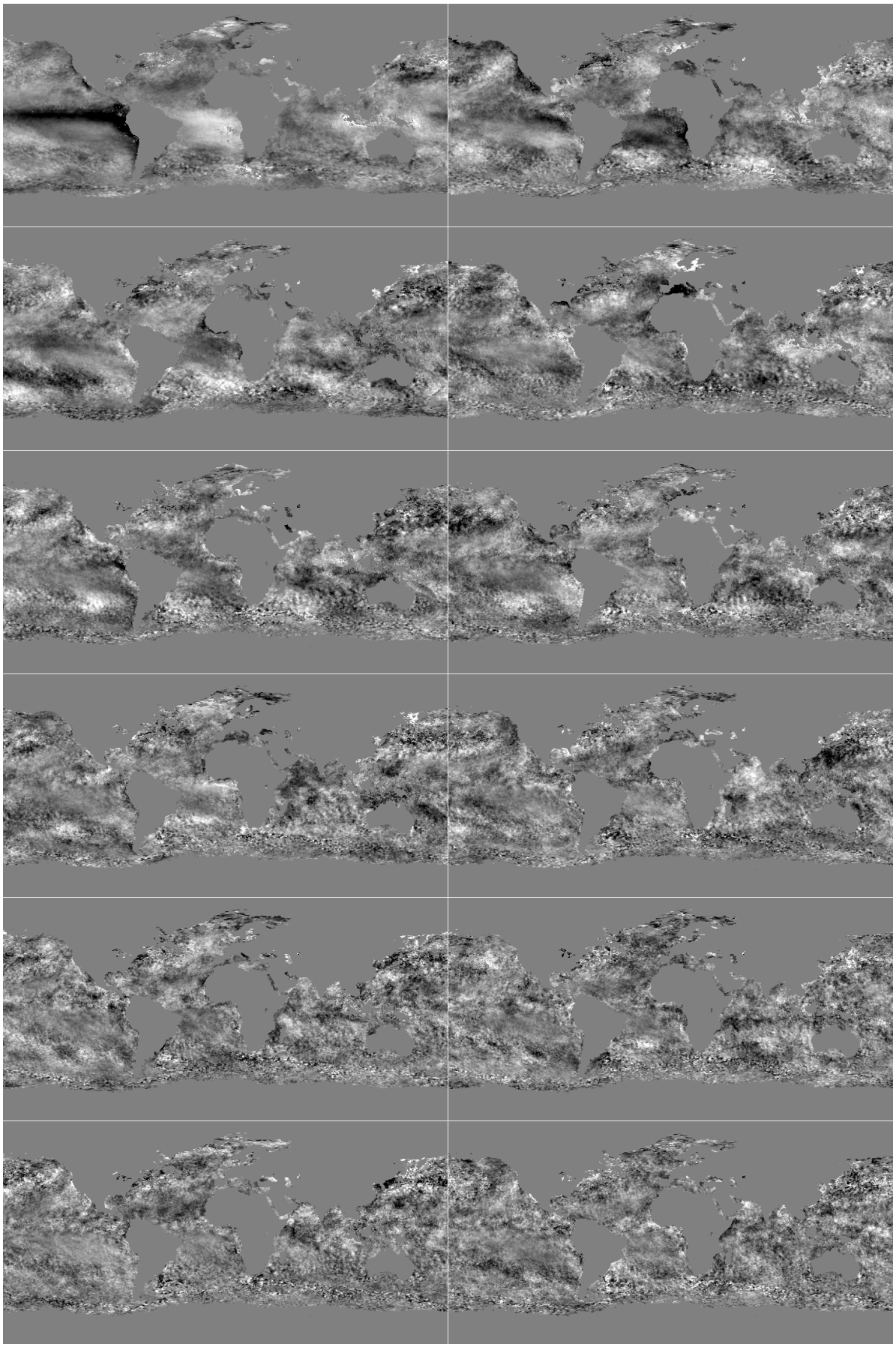

Fig. 3. MAF/MADs of 1996-1997 AVHRR monthly mean SST

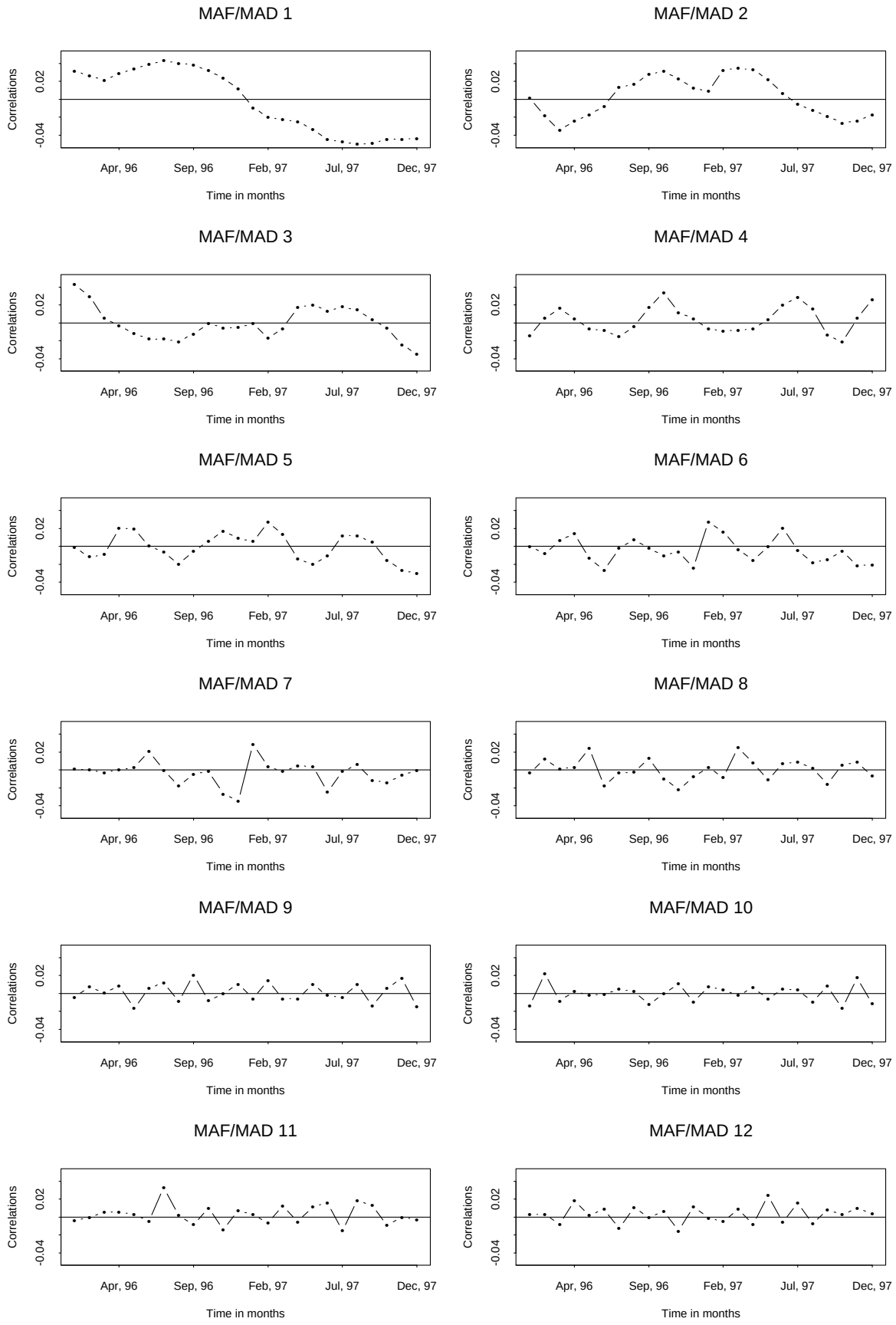

Fig. 4. Correlations between 1996-1997 AVHRR monthly mean SST and MAF/MADs